JOURNAL OF GUIDANCE, CONTROL, AND DYNAMICS
Vol. 31, No. 6, November–December 2008

Kalman Filter for Spinning Spacecraft Attitude Estimation

F. Landis Markley*
NASA Goddard Space Flight Center, Greenbelt, Maryland 20771
and
Joseph E. Sedlak†
a.i. solutions, Inc., Lanham, Maryland 20706

DOI: 10.2514/1.35221

This paper presents a Kalman filter using a seven-component attitude state vector comprising the angular momentum components in an inertial reference frame, the angular momentum components in the body frame, and a rotation angle. The relatively slow variation of these parameters makes this parameterization advantageous for spinning spacecraft attitude estimation. The filter accounts for the constraint that the magnitude of the angular momentum vector is the same in the inertial and body frames by employing a reduced six-component error state. Three variants of the filter, defined by different choices for the reduced error state, are tested against a quaternion-based filter using simulated data for the THEMIS mission. The infinitesimal attitude error angles are components of the error state in two of these variants, facilitating the computation of measurement sensitivity matrices and causing the usual 3 × 3 attitude covariance matrix to be a submatrix of the 6 × 6 covariance of the error state. These variants differ in their choice for the other three components of the error state, using either the angular momentum errors in the spacecraft body frame or in the inertial frame. The latter variant shows the best combination of robustness and efficiency in the simulations. Attitude estimation results using THEMIS flight data are also presented.

I. Introduction

ATTITUDE estimation is often more difficult for spinning spacecraft than for three-axis stabilized spacecraft. The parameters representing the spacecraft attitude and its time rate of change vary more rapidly in the spinning case, and gyro rate measurements are often lacking, requiring Euler's equations for modeling the attitude dynamics. This paper uses a seven-parameter angular-momentum-based representation that is advantageous for this application [1]. The seven state vector elements are the angular momentum components in an inertial reference frame, the angular momentum components in the spacecraft's body frame, and a rotation angle. These parameters are subject to the constraint that the magnitude of the angular momentum vector is the same in the inertial and body frames.

We have developed a series of extended Kalman filters (EKFs) employing this representation, to which we give the generic name SpinKF. The constraint on the state vector allows us to employ a six-component error state instead of the error vector of the full seven-component state, a procedure similar to the one commonly used to estimate the constrained four-component quaternion representation of attitude [2]. The conceptual advantages of this dimensional reduction, as more truly representing the actual degrees of freedom of the system, have been debated at length [3–9], but the computational advantages are indisputable. The different versions of SpinKF all use the same seven-component state but differ in their specification of the six-component error state. The first, SpinKF1 [10], was incorporated into the attitude ground support system for spinning spacecraft at the NASA Goddard Space Flight Center and used for operational support of the Space Technology 5 (ST5) mission [11–13]. A second version replaced SpinKF1 for early mission support of the Time History of Events and Macroscale Interaction During Substorms (THEMIS) mission [13,14]. These were superseded by two new implementations, SpinKF-B and SpinKF-I, which are the focus of this paper. In all the versions except SpinKF1, three of the components of the state error vector are the usual infinitesimal attitude error angles, making the usual 3×3 attitude covariance matrix a submatrix of the 6×6 covariance and greatly facilitating the computation of measurement sensitivity matrices.

The paper first introduces the seven-parameter angular-momentum-based representation and the method used to reduce the state error vector to six components. A derivation of the relation between the infinitesimal attitude error angles and the errors in the seven-component state follows, leading to an expression for the time derivative of the seventh component, the rotation angle. The general equations for the SpinKF Kalman filter are presented, and it is shown that all the computations can be performed in the reduced six-dimensional space, with the exception of the time propagation and measurement update of the state estimate. Complete derivations of SpinKF-B and SpinKF-I are provided in the body of the paper, and a brief introduction of SpinKF1 is given in the Appendix.

The error dynamics of SpinKF-I and SpinKF-B are analyzed by investigating the eigenvalues of their system dynamics matrices in the special case of constant angular momentum. The system dynamics are also compared with those of a more conventional EKF based on the quaternion and body rotation rate. We find that the error dynamics of all these filters have similar time dependence, involving both the spin rate and the body nutation rate. The SpinKF filters have an advantage over a quaternion-based filter in the state propagation itself, however, because the time derivative of the angular momentum in the body frame is proportional to the nutation frequency times the nutation amplitude, which is generally small. The time derivatives of the quaternion components, on the other hand, are proportional to the rotation frequency with no reduction by an amplitude factor.

This general presentation is followed by a discussion of details of the filter implementation, including measurement modeling and the method used to avoid a singularity in the angular-momentum-based attitude representation. Data simulated to represent the THEMIS spacecraft are then used to compare the performance of the three SpinKF variants and the quaternion-based EKF. Attitude estimation results using THEMIS flight data are presented and conclusions are drawn from the results of the simulations and flight data results.

Received 19 October 2007; revision received 25 January 2008; accepted for publication 26 January 2008.

*Aerospace Engineer, Guidance, Navigation, and Control Systems Engineering Branch, Code 591. Fellow AIAA.
†Senior Engineer, 10001 Derekwood Lane.

II. Angular-Momentum-Based Attitude Parameterization

The spacecraft's angular momentum about its center of mass expressed in its body frame, $\mathbf{L}_B$, or expressed in an inertial reference frame, $\mathbf{L}_I$, obeys the equations of motion [15]

$$\mathrm{d}\,\mathbf{L}_B/\mathrm{d}t = \mathbf{N}_B - \boldsymbol{\omega}_{BI} \times \mathbf{L}_B \tag{1a}$$

and

$$\mathrm{d}\,\mathbf{L}_I/\mathrm{d}t = \mathbf{N}_I = A_{BI}^T \mathbf{N}_B \tag{1b}$$

where $\mathbf{N}$ is the external torque, A_{BI} is the inertial-to-body attitude matrix, and the angular velocity $\boldsymbol{\omega}_{BI}$ is given by

$$\boldsymbol{\omega}_{BI} = J^{-1}(\mathbf{L}_B - \mathbf{L}_{\text{int}}) \tag{2}$$

In this equation J is the spacecraft moment-of-inertia tensor and $\mathbf{L}_{\text{int}}$ is the angular momentum relative to the spacecraft of any moving parts (reaction wheels, steerable antennas or solar arrays, flexible modes, fuel slosh, etc.). The angular momentum representations in the two different frames must obey the constraint

$$\|\mathbf{L}_B\| = \|\mathbf{L}_I\| \equiv L \tag{3}$$

where $\|\cdot\|$ denotes the Euclidean or 2-norm of a vector.

Spacecraft dynamics are commonly modeled by Eq. (1a) and kinematics by

$$\mathrm{d}\,A_{BI}/\mathrm{d}t = -[\boldsymbol{\omega}_{BI}\times]A_{BI} \tag{4}$$

where

$$[\mathbf{v}\times] \equiv \begin{bmatrix} 0 & -v_3 & v_2 \\ v_3 & 0 & -v_1 \\ -v_2 & v_1 & 0 \end{bmatrix} \tag{5}$$

denotes the cross-product matrix for an arbitrary three-component vector $\mathbf{v}$. A quaternion or some other lower-dimensional representation of A_{BI} is often integrated rather than Eq. (4), but this distinction is not important for this paper. An alternative formulation uses Eq. (1b) and

$$\mathbf{L}_B = A_{BI}\mathbf{L}_I \tag{6}$$

in place of Eq. (1a) [16]. For application to spinning spacecraft, this has the advantage that $\mathbf{L}_I$ varies more slowly than $\mathbf{L}_B$, but shares the disadvantage that the kinematic components of the state vector are fast variables.

The formulation in this paper is based on the Euler axis/angle representation of a rotation matrix [15,17]:

$$R(\mathbf{e},\phi) \equiv (\cos\phi)I_{3\times3} + (1-\cos\phi)\mathbf{e}\mathbf{e}^T - \sin\phi[\mathbf{e}\times] \tag{7}$$

where $\mathbf{e}$ is the axis and ϕ is the angle of rotation. Setting $\mathbf{e} = (\hat{\mathbf{L}}_B \times \hat{\mathbf{L}}_I)/\|\hat{\mathbf{L}}_B \times \hat{\mathbf{L}}_I\|$ and $\phi = \cos^{-1}(\hat{\mathbf{L}}_B \cdot \hat{\mathbf{L}}_I)$, where $\hat{\mathbf{L}}_I \equiv \mathbf{L}_I/L$ and $\hat{\mathbf{L}}_B \equiv \mathbf{L}_B/L$, gives the rotation matrix R_{BI} that takes $\hat{\mathbf{L}}_I$ to $\hat{\mathbf{L}}_B$ through the minimum rotation angle. This rotation matrix can be written, using the identity $[(\mathbf{u}\times\mathbf{v})\times] = \mathbf{v}\mathbf{u}^T - \mathbf{u}\mathbf{v}^T$, as

$$\begin{aligned} R_{BI} = {} & (\hat{\mathbf{L}}_B \cdot \hat{\mathbf{L}}_I)I_{3\times3} - \hat{\mathbf{L}}_I\hat{\mathbf{L}}_B^T + \hat{\mathbf{L}}_B\hat{\mathbf{L}}_I^T \\ & + (1 + \hat{\mathbf{L}}_B \cdot \hat{\mathbf{L}}_I)^{-1}(\hat{\mathbf{L}}_B \times \hat{\mathbf{L}}_I)(\hat{\mathbf{L}}_B \times \hat{\mathbf{L}}_I)^T \end{aligned} \tag{8}$$

Methods for dealing with the singularity of this expression when $\mathbf{L}_B$ and $\mathbf{L}_I$ are 180 deg apart will be discussed in Sec. VII. Because both the attitude matrix A_{BI} and the rotation matrix R_{BI} take the unit vector $\hat{\mathbf{L}}_I$ to $\hat{\mathbf{L}}_B$, the product $R_{BI}^T A_{BI}$ takes $\hat{\mathbf{L}}_I$ into itself, so it is a rotation about $\hat{\mathbf{L}}_I$ by some angle ζ and can be expressed as

$$R_{BI}^T A_{BI} = R(\hat{\mathbf{L}}_I, \zeta) \tag{9}$$

Multiplying both sides of Eq. (9) by R_{BI} gives

$$A_{BI} = R_{BI}R(\hat{\mathbf{L}}_I, \zeta) \tag{10}$$

Multiplying this equation on the right by $I_{3\times3} = R_{BI}^T R_{BI}$ and using the identity $R_{BI}R(\hat{\mathbf{L}}_I, \zeta)R_{BI}^T = R(\hat{\mathbf{L}}_B, \zeta)$ gives

$$A_{BI} = R(\hat{\mathbf{L}}_B, \zeta)R_{BI} \tag{11}$$

Either Eq. (10) or Eq. (11) gives our parameterization of the attitude matrix $A_{BI}(\mathbf{x})$ in terms of the seven-component state vector:

$$\mathbf{x} = [\,\mathbf{L}_B^T \quad \mathbf{L}_I^T \quad \zeta\,]^T \tag{12}$$

The dynamics are given by Eqs. (1a) and (1b) and a differential equation for ζ, derived in [1] and as Eq. (30) in this paper. SpinKF1 used a slightly different state vector, as described in the Appendix.

III. Reduction to a Six-Component Error State

A. General Considerations

A straightforward Kalman filter implementation would use the 7×7 covariance $P_x \equiv E\{(\Delta\mathbf{x})(\Delta\mathbf{x})^T\}$ of the error vector $\Delta\mathbf{x} \equiv \mathbf{x} - \bar{\mathbf{x}}$, where $\bar{\mathbf{x}} \equiv E\{\mathbf{x}\}$ is the expectation of $\mathbf{x}$. Note that an overbar will always denote an expectation. If the constraint of Eq. (3) were linear, P_x would be singular. However, because Eq. (3) is a nonlinear constraint analogous to the unity norm constraint of the four-component quaternion, we expect P_x to be ill-conditioned but not singular, as has been observed in the quaternion case [9]. As pointed out in [10], this means that all the useful covariance information can be contained in a well-conditioned matrix of rank six, in the same way that the quaternion norm constraint allows us to use a reduced-dimension covariance matrix [2]. In other words, in the context of extended Kalman filtering we can treat P_x as if it were singular, even though it is in fact only ill-conditioned. In the present case, the 7×7 covariance matrix P_x is assumed to have a null vector $\mathbf{x}_{\text{null}}$ that obeys

$$P_x\mathbf{x}_{\text{null}} = 0_{7\times1} \tag{13}$$

This is not really a null vector of the true covariance; it is in the direction of the eigenvector for which the eigenvalue leads to the ill-conditioning by being much smaller than the others.

The null vector must be orthogonal to all the vectors representing physically possible errors in $\mathbf{x}$. The six physically possible errors are a variation in ζ, two independent variations of $\mathbf{L}_B$ perpendicular to $\bar{\mathbf{L}}_B$, two variations of $\mathbf{L}_I$ perpendicular to $\bar{\mathbf{L}}_I$, and simultaneous length-changing equal-magnitude variations of $\mathbf{L}_B$ in the direction of $\bar{\mathbf{L}}_B$ and of $\mathbf{L}_I$ in the direction of $\bar{\mathbf{L}}_I$. Thus, the normalized null eigenvector of P_x must be

$$\mathbf{x}_{\text{null}} = \pm\frac{1}{\sqrt{2}}[\,\hat{\bar{\mathbf{L}}}_B^T \quad -\hat{\bar{\mathbf{L}}}_I^T \quad 0\,]^T \tag{14}$$

which is a vector of errors violating the norm constraint of Eq. (3).

We seek a 7×6 matrix S with Moore–Penrose pseudoinverse [18] S^+, which is uniquely defined such that

$$S^+S = I_{6\times6} \tag{15a}$$

$$SS^+ = I_{7\times7} - \mathbf{x}_{\text{null}}\mathbf{x}_{\text{null}}^T \tag{15b}$$

$$S^+\mathbf{x}_{\text{null}} = 0_{6\times1} \tag{15c}$$

Note that S and S^+ must be functions of expectations rather than true values, which are unknown by the estimator. The six-dimensional error vector

$$\Delta\mathbf{y} \equiv S^+\Delta\mathbf{x} \tag{16}$$

has a well-conditioned 6×6 error covariance P_y given by

$$P_y \equiv E\{(\Delta\mathbf{y})(\Delta\mathbf{y})^T\} = S^+P_x(S^+)^T \tag{17}$$

Because of Eqs. (13) and (15b), the 7×7 error covariance P_x can be recovered by

$$SP_yS^T = SS^+P_x(S^+)^TS^T = SS^+P_x(SS^+)^T = P_x \tag{18}$$

and the seven-component error vector, which must be orthogonal to $\mathbf{x}_{\text{null}}$, by

$$\Delta\mathbf{x} = I_{7\times7}\Delta\mathbf{x} = (SS^+ + \mathbf{x}_{\text{null}}\mathbf{x}_{\text{null}}^T)\Delta\mathbf{x} = S\Delta\mathbf{y} \tag{19}$$

B. Attitude Error Angles

The different varieties of SpinKF are distinguished by different choices for S^+. In all the SpinKF variants except SpinKF1, the upper three rows of the matrix S^+ are chosen so that the first three components of $\Delta\mathbf{y}$ are equal to the three attitude error angles in the body reference frame, $\Delta\boldsymbol{\theta}$. This choice results in the upper-left-hand corner of P_y being the usual 3×3 attitude error covariance, and we will see later that it also greatly facilitates computation of measurement sensitivity matrices.

The expression for $\Delta\boldsymbol{\theta}$ as a function of $\Delta\mathbf{x}$ can be found by computing the first-order increments of the attitude matrix with variations $\Delta\mathbf{L}_B$, $\Delta\mathbf{L}_I$, and $\Delta\zeta$ and using the relationship

$$\Delta A_{BI}(\mathbf{x}) = -[\Delta\boldsymbol{\theta}\times]A_{BI}(\mathbf{x}) \tag{20a}$$

$$[(\Delta\boldsymbol{\theta}_\zeta + \Delta\boldsymbol{\theta}_B + \Delta\boldsymbol{\theta}_I)\times] = -[A_{BI}(\mathbf{x}+\Delta\mathbf{x}) - A_{BI}(\mathbf{x})]A_{BI}^T(\mathbf{x}) \tag{20b}$$

Expanding this using Eq. (10) or Eq. (11) gives, suppressing the argument of A_{BI} for compactness,

$$[\Delta\boldsymbol{\theta}_\zeta\times] = -[R(\hat{\mathbf{L}}_B, \zeta+\Delta\zeta) - R(\hat{\mathbf{L}}_B, \zeta)]R^T(\hat{\mathbf{L}}_B, \zeta) \tag{21a}$$

$$[\Delta\boldsymbol{\theta}_B\times] = -[R_{BI}(\hat{\mathbf{L}}_B + \Delta\hat{\mathbf{L}}_B, \hat{\mathbf{L}}_I) - R_{BI}(\hat{\mathbf{L}}_B, \hat{\mathbf{L}}_I)]R_{BI}^T(\hat{\mathbf{L}}_B, \hat{\mathbf{L}}_I) \tag{21b}$$

$$[\Delta\boldsymbol{\theta}_I\times] = -R(\hat{\mathbf{L}}_B, \zeta)[R_{BI}(\hat{\mathbf{L}}_B, \hat{\mathbf{L}}_I + \Delta\hat{\mathbf{L}}_I) - R_{BI}(\hat{\mathbf{L}}_B, \hat{\mathbf{L}}_I)]A_{BI}^T \tag{21c}$$

It can be easily shown that

$$\Delta\boldsymbol{\theta}_\zeta = \hat{\mathbf{L}}_B\Delta\zeta \tag{22}$$

and with a great deal more difficulty that

$$\Delta\boldsymbol{\theta}_B = L^{-1}[-\hat{\mathbf{L}}_B \times \Delta\mathbf{L}_B - (\mathbf{w}\cdot\Delta\mathbf{L}_B)\hat{\mathbf{L}}_B] \tag{23}$$

where

$$\mathbf{w} \equiv (1 + \hat{\mathbf{L}}_B\cdot\hat{\mathbf{L}}_I)^{-1}(\hat{\mathbf{L}}_B\times\hat{\mathbf{L}}_I) = (L^2 + \mathbf{L}_B\cdot\mathbf{L}_I)^{-1}(\mathbf{L}_B\times\mathbf{L}_I) \tag{24}$$

The derivation of Eq. (23) uses the relationship

$$\Delta\hat{\mathbf{L}} = L^{-1}(I_{3\times3} - \hat{\mathbf{L}}\hat{\mathbf{L}}^T)\Delta\mathbf{L} \tag{25}$$

Equation (21c) can be written as

$$\begin{aligned}[(A_{BI}^T\Delta\boldsymbol{\theta}_I)\times] &= A_{BI}^T[\Delta\boldsymbol{\theta}_I\times]A_{BI} \\ &= -\{[R_{BI}^T(\hat{\mathbf{L}}_B, \hat{\mathbf{L}}_I + \Delta\hat{\mathbf{L}}_I) - R_{BI}^T(\hat{\mathbf{L}}_B, \hat{\mathbf{L}}_I)]R_{BI}(\hat{\mathbf{L}}_B, \hat{\mathbf{L}}_I)\}^T\end{aligned} \tag{26}$$

Comparison with Eqs. (8) and (21b) shows that $\Delta\boldsymbol{\theta}_I$ can be obtained from $\Delta\boldsymbol{\theta}_B$ by interchanging the subscripts B and I and multiplying by $-A_{BI}$, yielding

$$\Delta\boldsymbol{\theta}_I = L^{-1}[\hat{\mathbf{L}}_B\times(A_{BI}\Delta\mathbf{L}_I) - (\mathbf{w}\cdot\Delta\mathbf{L}_I)\hat{\mathbf{L}}_B] \tag{27}$$

Combining Eqs. (22), (23), and (27) gives the desired result

$$\begin{aligned}\Delta\boldsymbol{\theta} &= -L^{-1}\hat{\mathbf{L}}_B\times[\Delta\mathbf{L}_B - A_{BI}(\mathbf{x})\Delta\mathbf{L}_I] \\ &\quad + [\Delta\zeta - L^{-1}\mathbf{w}\cdot(\Delta\mathbf{L}_B + \Delta\mathbf{L}_I)]\hat{\mathbf{L}}_B\end{aligned} \tag{28}$$

which determines the first three rows of the matrix S^+.

Interpreting Eq. (28) as a relation of time variations of $\boldsymbol{\theta}$, $\mathbf{L}_B$, $\mathbf{L}_I$, and ζ gives

$$\begin{aligned}\boldsymbol{\omega}_{BI} &= -L^{-1}\hat{\mathbf{L}}_B\times\left[\frac{\mathrm{d}\mathbf{L}_B}{\mathrm{d}t} - A_{BI}(\mathbf{x})\frac{\mathrm{d}\mathbf{L}_I}{\mathrm{d}t}\right] \\ &\quad + \left[\frac{\mathrm{d}\zeta}{\mathrm{d}t} - L^{-1}\mathbf{w}\cdot\left(\frac{\mathrm{d}\mathbf{L}_B}{\mathrm{d}t} + \frac{\mathrm{d}\mathbf{L}_I}{\mathrm{d}t}\right)\right]\hat{\mathbf{L}}_B\end{aligned} \tag{29}$$

After substituting Eq. (1), Eq. (29) leads directly to the dynamic equation for ζ:

$$\begin{aligned}\mathrm{d}\zeta/\mathrm{d}t &= (1 + \hat{\mathbf{L}}_B\cdot\hat{\mathbf{L}}_I)^{-1}[(\hat{\mathbf{L}}_B + \hat{\mathbf{L}}_I)\cdot\boldsymbol{\omega}_{BI} \\ &\quad + L^{-1}(\hat{\mathbf{L}}_B\times\hat{\mathbf{L}}_I)\cdot(\mathbf{N}_B + \mathbf{N}_I)]\end{aligned} \tag{30}$$

C. SpinKF-B

SpinKF-B chooses the lower three rows of S^+ so that the last three components of $\Delta\mathbf{y}$ are equal to the components of the angular momentum error vector in the body reference frame. This is accomplished by setting

$$S_B^+ = \begin{bmatrix} \bar{L}^{-1}\{-[\hat{\bar{\mathbf{L}}}_B\times] - \hat{\bar{\mathbf{L}}}_B\bar{\mathbf{w}}^T\} & \bar{L}^{-1}\{[\hat{\bar{\mathbf{L}}}_B\times]A_{BI}(\bar{\mathbf{x}}) - \hat{\bar{\mathbf{L}}}_B\bar{\mathbf{w}}^T\} & \hat{\bar{\mathbf{L}}}_B \\ I_{3\times3} - \frac{1}{2}\hat{\bar{\mathbf{L}}}_B\hat{\bar{\mathbf{L}}}_B^T & \frac{1}{2}\hat{\bar{\mathbf{L}}}_B\hat{\bar{\mathbf{L}}}_I^T & 0_{3\times1} \end{bmatrix} \tag{31}$$

Then Eq. (16) gives

$$\Delta\mathbf{y}_B = \begin{bmatrix} \Delta\boldsymbol{\theta} \\ \Delta\mathbf{L}_B - \frac{1}{2}(\hat{\bar{\mathbf{L}}}_B\cdot\Delta\mathbf{L}_B - \hat{\bar{\mathbf{L}}}_I\cdot\Delta\mathbf{L}_I)\hat{\bar{\mathbf{L}}}_B \end{bmatrix} = \begin{bmatrix} \Delta\boldsymbol{\theta} \\ \Delta\mathbf{L}_B \end{bmatrix} \tag{32}$$

because $\hat{\bar{\mathbf{L}}}_B\cdot\Delta\mathbf{L}_B = \Delta L = \hat{\bar{\mathbf{L}}}_I\cdot\Delta\mathbf{L}_I$ for state errors that obey the angular momentum norm constraint. This $\Delta\mathbf{y}$ is closely related to the error state of a conventional EKF for a four-component quaternion and the angular velocity vector, using the techniques in [2] to handle the quaternion norm constraint. The pseudoinverse of S_B^+ is

$$S_B = \begin{bmatrix} 0_{3\times3} & I_{3\times3} \\ -A_{BI}^T(\bar{\mathbf{x}})[\bar{\mathbf{L}}_B\times] & A_{BI}^T(\bar{\mathbf{x}}) \\ [\hat{\bar{\mathbf{L}}}_B + \hat{\bar{\mathbf{L}}}_B\times A_{BI}(\bar{\mathbf{x}})\bar{\mathbf{w}}]^T & \bar{L}^{-1}[\bar{\mathbf{w}} + A_{BI}(\bar{\mathbf{x}})\bar{\mathbf{w}}]^T \end{bmatrix} \tag{33}$$

D. SpinKF-I

SpinKF-I chooses the lower three rows of S^+ so that the last three components of $\Delta\mathbf{y}$ are equal to the components of the angular momentum error vector in the inertial reference frame. The motivation for SpinKF-I is that $\Delta\mathbf{L}_I$ varies more slowly than $\Delta\mathbf{L}_B$ in the absence of torques, which should make the covariance propagation easier. The S^+ matrix in this case is

$$S_I^+ = \begin{bmatrix} \bar{L}^{-1}\{-[\hat{\bar{\mathbf{L}}}_B\times] - \hat{\bar{\mathbf{L}}}_B\bar{\mathbf{w}}^T\} & \bar{L}^{-1}\{[\hat{\bar{\mathbf{L}}}_B\times]A_{BI}(\bar{\mathbf{x}}) - \hat{\bar{\mathbf{L}}}_B\bar{\mathbf{w}}^T\} & \hat{\bar{\mathbf{L}}}_B \\ \frac{1}{2}\hat{\bar{\mathbf{L}}}_I\hat{\bar{\mathbf{L}}}_B^T & I_{3\times3} - \frac{1}{2}\hat{\bar{\mathbf{L}}}_I\hat{\bar{\mathbf{L}}}_I^T & 0_{3\times1} \end{bmatrix} \tag{34}$$

so Eq. (16) gives

$$\Delta \mathbf{y}_I = \begin{bmatrix} \Delta\boldsymbol{\theta} \\ \Delta \mathbf{L}_I + \frac{1}{2}(\hat{\bar{\mathbf{L}}}_B \cdot \Delta \mathbf{L}_B - \hat{\bar{\mathbf{L}}}_I \cdot \Delta \mathbf{L}_I)\hat{\bar{\mathbf{L}}}_I \end{bmatrix} = \begin{bmatrix} \Delta\boldsymbol{\theta} \\ \Delta \mathbf{L}_I \end{bmatrix} \quad (35)$$

The pseudoinverse of S_I^+ is

$$S_I = \begin{bmatrix} [\bar{\mathbf{L}}_B\times] & A_{BI}(\bar{\mathbf{x}}) \\ 0_{3\times 3} & I_{3\times 3} \\ (\hat{\bar{\mathbf{L}}}_B - \hat{\bar{\mathbf{L}}}_B \times \bar{\mathbf{w}})^T & \bar{L}^{-1}[\bar{\mathbf{w}} + A_{BI}^T(\bar{\mathbf{x}})\bar{\mathbf{w}}]^T \end{bmatrix} \quad (36)$$

IV. Kalman Filter Formulation

A. Kalman Gain and Covariance Update

A Kalman filter for the seven-component state vector $\mathbf{x}$ uses Eqs. (1) and (30) to propagate the state estimate between observations. The filter update for a measurement $\mathbf{z} = \mathbf{h}(\mathbf{x})$ is given by [19]

$$\mathbf{x}(+) = \mathbf{x}(-) + K_x[\tilde{\mathbf{z}} - \mathbf{h}(-)] \quad (37)$$

where the arguments $(-)$ and $(+)$ denote estimates before and after the update, respectively; $\tilde{\mathbf{z}}$ denotes the measured value; $\mathbf{h}(-) \equiv \mathbf{h}(\mathbf{x}(-))$; and K_x is the Kalman gain. The gain is given by

$$K_x = P_x(-)H_x^T[H_x P_x(-)H_x^T + R]^{-1} \quad (38)$$

where the measurement sensitivity matrix is

$$H_x \equiv \frac{\partial \mathbf{h}(\mathbf{x})}{\partial \mathbf{x}} \quad (39)$$

and R is the measurement error covariance. The covariance is updated by

$$P_x(+) = (I_{7\times 7} - K_x H_x)P_x(-) \quad (40)$$

To avoid using an ill-conditioned covariance matrix, we substitute Eq. (18) into Eq. (38), giving

$$K_x = S(-)K_y \quad (41)$$

where the matrix S must be evaluated with the preupdate estimate and where K_y is given by

$$K_y = P_y(-)H_y^T[H_y P_y(-)H_y^T + R]^{-1} \quad (42)$$

with

$$H_y \equiv H_x S(-) = \frac{\partial \mathbf{h}(\mathbf{x})}{\partial \mathbf{x}}\frac{\partial \mathbf{x}}{\partial(\Delta\mathbf{y})} = \frac{\partial \mathbf{h}}{\partial(\Delta\mathbf{y})} \quad (43)$$

Substituting Eqs. (18) and (41) into Eq. (40) and using Eq. (43) gives

$$S(+)P_y(+)S^T(+) = S(-)(I_{6\times 6} - K_y H_y)P_y(-)S^T(-) \quad (44)$$

Ignoring the higher-order difference between $S(+)$ and $S(-)$ gives

$$P_y(+) = (I_{6\times 6} - K_y H_y)P_y(-) \quad (45)$$

Reynolds [20] has addressed the validity of this assumption. Note that with this approximation the matrix S^+ does not appear in the final formulation of the EKF, and S appears only in the state update via Eq. (41).

B. State Update: SpinKF-B

The state update in SpinKF-B is given by

$$\mathbf{x}(+) = \mathbf{x}(-) + S_B K_y[\tilde{\mathbf{z}} - \mathbf{h}(-)] \equiv \mathbf{x}(-) + S_B\begin{bmatrix} \Delta\bar{\boldsymbol{\theta}} \\ \Delta\bar{\mathbf{L}}_B \end{bmatrix} \quad (46)$$

Substituting $S_B(-)$ from Eq. (33) gives

$$\bar{\mathbf{L}}_B(+) = \bar{\mathbf{L}}_B(-) + \Delta\bar{\mathbf{L}}_B \quad (47a)$$

$$\begin{aligned}\bar{\mathbf{L}}_I(+) &= \bar{\mathbf{L}}_I(-) + A_{BI}^T(-)[\Delta\bar{\mathbf{L}}_B + \Delta\bar{\boldsymbol{\theta}} \times \bar{\mathbf{L}}_B(-)] \\ &= A_{BI}^T(-)[\bar{\mathbf{L}}_B(-) + \Delta\bar{\mathbf{L}}_B + \Delta\bar{\boldsymbol{\theta}} \times \bar{\mathbf{L}}_B(-)]\end{aligned} \quad (47b)$$

The update preserves the norm constraint of Eq. (3) to first order but violates it in second order, as in the quaternion case [2]. The cross-product term in Eq. (47b) appears to be the first-order approximation to a rotation, and so we trust the magnitude of $\bar{\mathbf{L}}_B(+)$ more than that of $\bar{\mathbf{L}}_I(+)$ and renormalize the latter by

$$\bar{\mathbf{L}}_I(++) = \|\bar{\mathbf{L}}_B(+)\|\hat{\bar{\mathbf{L}}}_I(+) \quad (48)$$

to restore the norm constraint.

C. State Update: SpinKF-I

The state update in SpinKF-I is given by

$$\mathbf{x}(+) = \mathbf{x}(-) + S_I(-)K_y[\tilde{\mathbf{z}} - \mathbf{h}(-)] \equiv \mathbf{x}(-) + S_I(-)\begin{bmatrix} \Delta\bar{\boldsymbol{\theta}} \\ \Delta\bar{\mathbf{L}}_I \end{bmatrix} \quad (49)$$

Substituting $S_I(-)$ from Eq. (36) gives

$$\begin{aligned}\bar{\mathbf{L}}_B(+) &= \bar{\mathbf{L}}_B(-) - \Delta\bar{\boldsymbol{\theta}} \times \bar{\mathbf{L}}_B(-) + A_{BI}(-)\Delta\bar{\mathbf{L}}_I \\ &= A_{BI}(-)[\bar{\mathbf{L}}_I(-) + \Delta\bar{\mathbf{L}}_I] - \Delta\bar{\boldsymbol{\theta}} \times \bar{\mathbf{L}}_B(-)\end{aligned} \quad (50a)$$

$$\bar{\mathbf{L}}_I(+) = \bar{\mathbf{L}}_I(-) + \Delta\bar{\mathbf{L}}_I \quad (50b)$$

which also violates the norm constraint in second order. Because the cross-product term occurs in Eq. (50a), the norm constraint in SpinKF-I is restored by

$$\bar{\mathbf{L}}_B(++) = \|\bar{\mathbf{L}}_I(+)\|\hat{\bar{\mathbf{L}}}_B(+) \quad (51)$$

D. Covariance Propagation

The matrices F_y and G_y in the covariance propagation equation

$$\mathrm{d}P_y/\mathrm{d}t = F_y P_y + P_y F_y^T + G_y Q G_y^T \quad (52)$$

are most easily computed directly from the equations for the reduced state error vector $\Delta\mathbf{y}$. We assume that

$$\mathbf{N}_B = \bar{\mathbf{N}}_B + J\mathbf{n}_u \quad (53a)$$

and

$$\mathbf{L}_{\text{int}} = \bar{\mathbf{L}}_{\text{int}} - J\mathbf{n}_v \quad (53b)$$

where the overbars denote a priori expectations and where $\mathbf{n}_u$ and $\mathbf{n}_v$ are assumed to be independent zero-mean Gaussian white noise processes with

$$\begin{aligned}&E\left\{\begin{bmatrix} \mathbf{n}_v(t) \\ \mathbf{n}_u(t) \end{bmatrix}\begin{bmatrix} \mathbf{n}_v(t') \\ \mathbf{n}_u(t') \end{bmatrix}^T\right\} \\ &\quad = Q(t)\delta(t-t') = \begin{bmatrix} Q_v(t) & 0_{3\times 3} \\ 0_{3\times 3} & Q_u(t) \end{bmatrix}\delta(t-t')\end{aligned} \quad (54)$$

where $\delta(t-t')$ is the Dirac delta function. The definitions in Eq. (53) are arranged so that $\mathbf{n}_u$ and $\mathbf{n}_v$ have dimensions of angular acceleration and angular velocity, respectively, and Q_u and Q_v have units of $\mathrm{rad}^2/\mathrm{s}^3$ and $\mathrm{rad}^2/\mathrm{s}$. Note that Q_v may be nonzero even for a nominally rigid spacecraft.

To first order, the attitude error vector obeys the dynamics equation (17):

$$\mathrm{d}(\Delta\boldsymbol{\theta})/\mathrm{d}t = \Delta\boldsymbol{\omega}_{BI} - \bar{\boldsymbol{\omega}}_{BI} \times \Delta\boldsymbol{\theta} \quad (55)$$

For SpinKF-B, we need the dynamics equation obeyed by the angular momentum error in the body frame:

$$\begin{aligned} \mathrm{d}(\Delta\mathbf{L}_B)/\mathrm{d}t &= \Delta[\mathbf{N}_B - \boldsymbol{\omega}_{BI} \times \mathbf{L}_B] \\ &= \bar{\mathbf{L}}_B \times \Delta\boldsymbol{\omega}_{BI} - \bar{\boldsymbol{\omega}}_{BI} \times \Delta\mathbf{L}_B + J\mathbf{n}_u \end{aligned} \tag{56}$$

From Eq. (2) we have

$$\Delta\boldsymbol{\omega}_{BI} = J^{-1}(\Delta\mathbf{L}_B - \Delta\mathbf{L}_{\mathrm{int}}) = J^{-1}\Delta\mathbf{L}_B + \mathbf{n}_v \tag{57}$$

and so differentiating Eq. (32) gives

$$\frac{\mathrm{d}(\Delta\mathbf{y}_B)}{\mathrm{d}t} = F_{yB}\Delta\mathbf{y}_B + G_{yB}\begin{bmatrix}\mathbf{n}_v \\ \mathbf{n}_u\end{bmatrix} \tag{58}$$

with

$$F_{yB} \equiv \begin{bmatrix} -[\bar{\boldsymbol{\omega}}_{BI}\times] & J^{-1} \\ 0_{3\times3} & [\bar{\mathbf{L}}_B\times]J^{-1} - [\bar{\boldsymbol{\omega}}_{BI}\times] \end{bmatrix} \tag{59a}$$

and

$$G_{yB} \equiv \begin{bmatrix} I_{3\times3} & 0_{3\times3} \\ [\bar{\mathbf{L}}_B\times] & J \end{bmatrix} \tag{59b}$$

SpinKF-I uses the dynamics equation obeyed by the angular momentum error in the inertial frame

$$\begin{aligned} \mathrm{d}(\Delta\mathbf{L}_I)/\mathrm{d}t &= \Delta\mathbf{N}_I = \Delta[A_{BI}^T(\mathbf{x})\mathbf{N}_B] \\ &= \Delta\{A_{BI}^T(\bar{\mathbf{x}})(I_{3\times3} + [\Delta\boldsymbol{\theta}\times])(\bar{\mathbf{N}}_B + J\mathbf{n}_u)\} \\ &= A_{BI}^T(\bar{\mathbf{x}})(J\mathbf{n}_u - \bar{\mathbf{N}}_B \times \Delta\boldsymbol{\theta}) \end{aligned} \tag{60}$$

We also use Eqs. (2), (6), and (20a) to obtain

$$\begin{aligned} \Delta\boldsymbol{\omega}_{BI} &= J^{-1}\Delta[A_{BI}(\mathbf{x})\mathbf{L}_I - \mathbf{L}_{\mathrm{int}}] \\ &= J^{-1}\{-[\Delta\boldsymbol{\theta}\times]A_{BI}(\bar{\mathbf{x}})\bar{\mathbf{L}}_I + A_{BI}(\bar{\mathbf{x}})\Delta\mathbf{L}_I - \Delta\mathbf{L}_{\mathrm{int}}\} \\ &= J^{-1}[\bar{\mathbf{L}}_B \times \Delta\boldsymbol{\theta} + A_{BI}(\bar{\mathbf{x}})\Delta\mathbf{L}_I] + \mathbf{n}_v \end{aligned} \tag{61}$$

An equation analogous to Eq. (58) is obtained for SpinKF-I with

$$F_{yI} \equiv \begin{bmatrix} J^{-1}[\bar{\mathbf{L}}_B\times] - [\bar{\boldsymbol{\omega}}_{BI}\times] & J^{-1}A_{BI}(\bar{\mathbf{x}}) \\ -A_{BI}^T(\bar{\mathbf{x}})[\bar{\mathbf{N}}_B\times] & 0_{3\times3} \end{bmatrix} \tag{62a}$$

and

$$G_{yI} \equiv \begin{bmatrix} I_{3\times3} & 0_{3\times3} \\ 0_{3\times3} & A_{BI}^T(\bar{\mathbf{x}})J \end{bmatrix} \tag{62b}$$

V. Error State Dynamics

The F_y matrix contains important information about the filter dynamics. In particular, if F_y is constant, its eigenvalues give the characteristic rates of change of the error states. Therefore, in this section, we will examine the special case that $\bar{\boldsymbol{\omega}}_{BI}$ and $\bar{\mathbf{L}}_B$ are constant, which means that $\bar{\mathbf{L}}_{\mathrm{int}}$ is constant and that the right side of Eq. (1a) is zero. Cancellation of the two terms on the right side of this equation is possible but highly unlikely, and so we will assume that both $\bar{\mathbf{N}}_B$ and $\bar{\boldsymbol{\omega}}_{BI} \times \bar{\mathbf{L}}_B$ are zero. The cross-product condition means that

$$\bar{\mathbf{L}}_B = \gamma\bar{\boldsymbol{\omega}}_{BI} \tag{63}$$

for some constant scalar γ, so that

$$F_{yB} = \begin{bmatrix} -[\bar{\boldsymbol{\omega}}_{BI}\times] & J^{-1} \\ 0_{3\times3} & [\bar{\boldsymbol{\omega}}_{BI}\times](\gamma J^{-1} - I_{3\times3}) \end{bmatrix} \tag{64}$$

and

$$F_{yI} = \begin{bmatrix} (\gamma J^{-1} - I_{3\times3})[\bar{\boldsymbol{\omega}}_{BI}\times] & J^{-1}A_{BI}(\bar{\mathbf{x}}) \\ 0_{3\times3} & 0_{3\times3} \end{bmatrix} \tag{65}$$

The eigenvalues of a block triangular matrix are the eigenvalues of the blocks on the diagonal. The characteristic equation of the 3×3 blocks on the diagonal of Eqs. (64) and (65) is

$$\begin{aligned} 0 = \det(\lambda I_{3\times3} - M) &= \lambda^3 - \lambda^2 \operatorname{tr} M + \lambda \operatorname{tr}(\operatorname{adj} M) - \det M \\ &= \lambda[\lambda^2 + \operatorname{tr}(\operatorname{adj} M)] \end{aligned} \tag{66}$$

where $\det(\cdot)$, $\operatorname{tr}(\cdot)$, and $\operatorname{adj}(\cdot)$ denote the matrix determinant, trace, and adjoint (or adjugate; that is, the transposed matrix of cofactors). The final equality in Eq. (66) follows from the vanishing of the trace and determinant of the 3×3 matrices in question. We use the invariance of the trace of a matrix product under cyclic permutation of its factors and the identities $\operatorname{adj}(AB) = (\operatorname{adj}B)(\operatorname{adj}A)$ and $\operatorname{adj}([\boldsymbol{\omega}\times]) = \boldsymbol{\omega}\boldsymbol{\omega}^T$ to evaluate $\operatorname{tr}(\operatorname{adj}M)$. This gives the eigenvalues of F_{yB} as 0 (twofold degenerate), $\pm i\omega$, and $\pm i\omega_n$, where $\omega \equiv \|\boldsymbol{\omega}\|$ and the body nutation rate ω_n is

$$\omega_n = \pm[\boldsymbol{\omega}^T \operatorname{adj}(\gamma J^{-1} - I_{3\times3})\boldsymbol{\omega}]^{1/2} \tag{67}$$

The eigenvalues of F_{yI} are 0 (fourfold degenerate) and $\pm i\omega_n$, which would indicate that the error dynamics of SpinKF-I are more benign than those of SpinKF-B. This could have been anticipated without computing the eigenvalues by noting the presence of the zero matrix in the lower-right corner of Eq. (62a). Equation (4) shows, though, that the spin rate ω enters F_{yI} through the attitude matrix in the offdiagonal block of Eq. (65), and so the advantage of SpinKF-I is not clear-cut.

If $\bar{\mathbf{L}}_{\mathrm{int}}$ is not zero, Eq. (63) can be satisfied for steady rotation about an axis that is not a principal axis of inertia. We now turn to the special case that the internal angular momentum is zero, and so Eq. (63) requires the rotation to be about a principal axis. Let $J = \operatorname{diag}([J_1, J_2, J_3])$ and assume that the rotation is about the third axis. Then $\gamma = J_3$ and Eq. (67) gives

$$\omega_n = \pm[(1 - J_3/J_1)(1 - J_3/J_2)]^{1/2}\omega \tag{68}$$

This is the expected result, giving unstable motion, indicated by pure imaginary ω_n, if J_3 is the intermediate moment of inertia. If J_3 is the maximum or minimum principal moment of inertia, Eq. (68) gives periodic motion with real ω_n. If, in addition, $J_1 = J_2$, we see that

$$\omega_n = (1 - J_3/J_1)\omega \tag{69}$$

which is the usual expression for the body nutation rate, with the conventional sign [15].

VI. Relation to a Quaternion-Based EKF

The SpinKF filters have been tested against the unit vector filter (UVF) [21], which has supported many three-axis stabilized spacecraft at NASA Goddard Space Flight Center over the past 16 years. For application to spinning spacecraft, the UVF was modified to estimate the quaternion and rotation rate rather than the gyro biases, to use dynamics propagation rather than gyro propagation, and to use linearized dynamics matrices for covariance propagation. The UVF represents the attitude by a quaternion, but employs the six-component error state $\Delta\mathbf{y}_{\theta\omega}$ comprising the three attitude error angles and the errors in the angular velocity vector. For a simple spinner with no internal angular momentum, this error state vector is simply related to the SpinKF-B error state vector by

$$\Delta\mathbf{y}_B = \begin{bmatrix} \Delta\boldsymbol{\theta} \\ J\Delta\boldsymbol{\omega}_{BI} \end{bmatrix} = C_B\Delta\mathbf{y}_{\theta\omega} \tag{70}$$

where

$$C_B \equiv \begin{bmatrix} I_{3\times3} & 0_{3\times3} \\ 0_{3\times3} & J \end{bmatrix} \tag{71}$$

The SpinKF-B and SpinKF-I error states are related by

$$\Delta\mathbf{y}_I = S_I^+ \Delta\mathbf{x} = S_I^+ S_B \Delta\mathbf{y}_B = \begin{bmatrix} I_{3\times3} & O_{3\times3} \\ -A_{BI}^T(\bar{\mathbf{x}})[\bar{\mathbf{L}}_B\times] & A_{BI}^T(\bar{\mathbf{x}}) \end{bmatrix} \Delta\mathbf{y}_B \tag{72}$$

So the relation between the UVF error state vector and the SpinKF-I error state vector is

$$\Delta\mathbf{y}_I = C_I \Delta\mathbf{y}_{\theta\omega} \tag{73}$$

with

$$C_I \equiv \begin{bmatrix} I_{3\times3} & 0_{3\times3} \\ -A_{BI}^T(\bar{\mathbf{x}})[\bar{\mathbf{L}}_B\times] & A_{BI}^T(\bar{\mathbf{x}})J \end{bmatrix} \tag{74}$$

The UVF covariance $P_{\theta\omega}$ is thus related to the SpinKF-I covariance by

$$P_{yI} = C_I P_{\theta\omega} C_I^T \tag{75a}$$

$$P_{\theta\omega} = C_I^{-1} P_{yI} (C_I^{-1})^T \tag{75b}$$

Analogous equations hold for the transformations between $P_{\theta\omega}$ and P_{yB}.

Note that because C_B is a constant, the dynamic matrices of the UVF are related to those of SpinKF-B by

$$F_{\theta\omega} = C_B^{-1} F_{yB} C_B \tag{76a}$$

and

$$G_{\theta\omega} = C_B^{-1} G_{yB} \tag{76b}$$

One consequence of Eq. (76a) is that the eigenvalues of $F_{\theta\omega}$ are the same as those of F_{yB}, under the conditions assumed in Sec. V.

VII. Filter Implementation

All the versions of SpinKF and the UVF modified as described in Sec. VI were implemented in MATLAB™ and built into a simulator/testbed designed specifically for comparing filter performance and capable of modeling spinning spacecraft with a wide variety of sensor types and several torque scenarios. SpinKF-I has now been incorporated as the EKF subsystem of the NASA Goddard Space Flight Center's Multimission Spin Axis Stabilized Spacecraft Attitude Ground Support System, adding the capability to solve for a time-dependent attitude history. This can be used for real-time applications, if needed. The software processes sensor data and presents it to the filter as vector observations. After discarding outliers, SpinKF-I integrates the state vector and its covariance to the next observation time using a fourth-order Runge–Kutta integrator with an appropriate time step. The filter obtains the spacecraft ephemeris and geomagnetic field and computes torques due to gravity gradients and any residual constant spacecraft magnetization at each integration step [15]. Control torques, if known, can be included. Then the sensor residual and the sensitivity matrix are computed, and the state and covariance are updated using the symmetric Joseph form [19] for the covariance update in place of Eq. (45).

A. Measurement Models

It is easier to calculate the measurement sensitivity matrices directly from the six-component error vector $\Delta\mathbf{y}$ than from the seven-component state vector $\mathbf{x}$. For a vector measurement, $\mathbf{z} = \mathbf{v}_B$ and

$$\mathbf{h}(\mathbf{x}) = A_{BI}(\mathbf{x})\mathbf{v}_I \simeq (I_{3\times3} - [\Delta\boldsymbol{\theta}\times])A_{BI}(\bar{\mathbf{x}})\mathbf{v}_I = \bar{\mathbf{v}}_B + \bar{\mathbf{v}}_B \times \Delta\boldsymbol{\theta} \tag{77}$$

where

$$\bar{\mathbf{v}}_B \equiv A_{BI}(\bar{\mathbf{x}})\mathbf{v}_I \tag{78}$$

It follows from Eq. (32) or Eq. (35) and the rightmost part of Eq. (43) that

$$H_y^{\text{vector}} = [\,[\bar{\mathbf{v}}_B\times] \quad 0_{3\times3}\,] \tag{79}$$

In the case of quaternion measurements, such as those output from an autonomous star tracker, an error quaternion is defined as the quotient of a preupdate quaternion $q(-)$ and the observed quaternion rotated into the body frame:

$$\Delta q = [\,\Delta\mathbf{q}^T \quad \Delta q_4\,]^T = q(-) \otimes q_{\text{obs}}^{-1} \tag{80}$$

This computation uses the quaternion multiplication convention of [2] that gives $A(q \otimes q') = A(q)A(q')$. Then the observation residual is given by

$$\tilde{\mathbf{z}} - \mathbf{h}(-) \equiv -2\text{sign}(\Delta q_4)\|\Delta\mathbf{q}\|^{-1}\sin^{-1}(\|\Delta\mathbf{q}\|)\Delta\mathbf{q} \tag{81}$$

and the measurement sensitivity matrix is simply

$$H_y^{\text{quaternion}} = [\,I_{3\times3} \quad 0_{3\times3}\,] \tag{82}$$

The preupdate quaternion can be extracted from $A_{BI}(-)$ by the usual method [15] or computed directly from $\mathbf{x}(-)$ by [1,22,23]

$$q(\mathbf{x}) = [2(1 + \hat{\mathbf{L}}_B \cdot \hat{\mathbf{L}}_I)]^{-1/2} \times \begin{bmatrix} \cos(\zeta/2)(\hat{\mathbf{L}}_B \times \hat{\mathbf{L}}_I) + \sin(\zeta/2)(\hat{\mathbf{L}}_B + \hat{\mathbf{L}}_I) \\ \cos(\zeta/2)(1 + \hat{\mathbf{L}}_B \cdot \hat{\mathbf{L}}_I) \end{bmatrix} \tag{83}$$

The quaternion can also be used to implement a linear observation model for vector measurements [20], but that model has not been employed in this work.

For spacecraft with gyros, the gyro outputs are used as measurements to update the state, rather than being used for state propagation in model replacement mode [2]. The gyro sensitivity matrix is the only measurement sensitivity matrix that is different between SpinKF-B and SpinKF-I. The gyro measurement model is

$$\mathbf{h}(\mathbf{x}) = UJ^{-1}(\mathbf{L}_B - \mathbf{L}_{\text{int}}) \tag{84}$$

where the rows of U are the gyro-sensitive axes in the body frame. Thus, in SpinKF-B, we have simply

$$H_{yB}^{\text{gyro}} = U[\,0_{3\times3} \quad J^{-1}\,] \tag{85}$$

In SpinKF-I, on the other hand, $H_x^{\text{gyro}} = U[\,J^{-1} \quad 0_{3\times3} \quad 0_{3\times1}\,]$, which yields

$$H_{yI}^{\text{gyro}} = H_x^{\text{gyro}} S_I(-) = UJ^{-1}[\,[\bar{\mathbf{L}}_B\times] \quad A_{BI}(\bar{\mathbf{x}})\,] \tag{86}$$

B. Singularity Avoidance

It is clear throughout the development of this filter that the spacecraft angular momentum is required to be nonzero and that the algorithm is also singular when $\hat{\mathbf{L}}_B$ and $\hat{\mathbf{L}}_I$ are 180 deg apart. The software checks for the latter singular condition and redefines the inertial reference frame so that $\hat{\mathbf{L}}_I$ is always greater than a user-specified distance from $-\hat{\mathbf{L}}_B$ in the modified frame, transforming all reference vectors along with $\hat{\mathbf{L}}_I$. Reconstructing the attitude referenced to the standard inertial frame is only a matter of keeping track of these reference frame rotations, which are all handled internally and are totally transparent to the user of the software.

The tolerance for avoiding the singularity was set to 20 deg in all the test cases. Thus, whenever the inner product of $\hat{\mathbf{L}}_I$ and $\hat{\mathbf{L}}_B$ is less than cos(160 deg), the inertial frame is redefined to put $\hat{\mathbf{L}}_I$ as far from $-\hat{\mathbf{L}}_B$ as possible. That is, in the new inertial frame, $\hat{\mathbf{L}}_I$ becomes numerically equal to $\hat{\mathbf{L}}_B$. The transformation matrix is constructed as the rotation by the angle from $\hat{\mathbf{L}}_I$ to $\hat{\mathbf{L}}_B$ about the axis $\hat{\mathbf{L}}_B \times \hat{\mathbf{L}}_I$. In

these computations, $\hat{\mathbf{L}}_B$ is simply a triad of numbers, treated as an independent vector in the inertial frame and without concern for the fact that it actually represents the same physical vector as $\hat{\mathbf{L}}_I$. The matrices so constructed are accumulated so that the software always can transform the reference vectors, typically defined in a standard J2000 Earth-centered inertial frame, into the body frame for use during the filter update step.

The covariance for SpinKF-I must also be transformed when the inertial frame is redefined. This is accomplished in two steps. The first step is to obtain the covariance for the simple body-frame attitude and rate error, $P_{\theta\omega}$, from the SpinKF-I covariance using Eq. (75b), where the $A_{BI}(\bar{\mathbf{x}})$ in C_I here refers to the attitude transformation from the previously defined inertial frame to the body frame. Then the SpinKF-I covariance in the new frame is constructed using Eq. (75a), where the $A_{BI}(\bar{\mathbf{x}})$ in C_I now refers to the attitude transformation from the redefined inertial frame to the body frame.

VIII. Testing with Simulated Data

A. Simulation Parameters

All the key features of the different versions of SpinKF and of the UVF were exercised in tests using simulation parameters based on the THEMIS series of spinning spacecraft [14]. THEMIS, launched on 17 February 2007, consists of five identical probes designed to study magnetic substorms in the Earth's magnetosphere. The initial orbit for all five probes had an inclination of about 14 deg, period of 31 h, and eccentricity of 0.85, giving perigee and apogee heights of roughly 900 and 87,000 km, respectively. The simulations used this orbit and the initial release spin direction that had a right ascension of 51.3 deg and declination of −23.2 deg. The probes have since been maneuvered into orbits with periods and phasing that cause them to line up radially from the Earth at apogee once every four days, and the spin axes have all been oriented along the normal to the ecliptic plane.

The probes are low-mass (126 kg), spin-stabilized at 20 rpm about the body Z axis, and carry single-head slit-type sun sensors and three-axis magnetometers (TAM) for attitude determination. The slit sun sensor measures the sun angle from the Z axis once per spin and generates a timing pulse. The ground software constructs a body-frame sun vector from the measured angle and the known slit azimuth. The TAM measurement frequency used for attitude determination is 8 Hz, which gives a generous 24 observations per spin period.

The TAM is both an attitude sensor and a science instrument, and its inherent noise is very small (0.01 nT). Thus, the TAM error for attitude determination is almost entirely due to errors in the reference field, which is modeled by the International Geomagnetic Reference Field (IGRF). The errors in the IGRF are time-correlated and can be modeled by adding magnetic field error parameters to the estimation state vector [24]. This additional complexity is generally avoided by using a suboptimal white noise model with standard deviations large enough to account for the non-Gaussian errors [16,25,26]. Both our simulations and filters modeled the TAM errors as Gaussian errors with standard deviation of 100 nT on each axis.

The sun sensor errors are due to a combination of sun angle measurement error and sun pulse timing error. They were modeled as Gaussian errors with standard deviation of 0.16 deg per axis.

The inertia tensor used for all the simulations is

$$J = \text{diag}([13, 13, 22])\ \text{kg-m}^2 \tag{87}$$

This value is of the correct magnitude for THEMIS after deployment of the TAM boom but before deployment of the long wire radial booms. The tensor was taken to be axisymmetric to simplify computation of simulated attitudes. Note that with this inertia tensor, Eq. (69) gives $\omega_n = -0.69\omega$, and so the dynamics of SpinKF-I are not significantly slower than those of SpinKF-B or the UVF. Thus, THEMIS does not show the SpinKF filters to best advantage.

A nutation angle of 2 deg was assumed in all the torque-free runs. The simulator and the filter propagation routine allow for environmental torques, but these were turned off for the tests presented here. The process noise was taken to be

$$Q_v = 10^{-6}\ \text{rad}^2/\text{s} \times \text{diag}([1, 1, 3]) \tag{88a}$$

$$Q_u = 10^{-7}\ \text{rad}^2/\text{s}^3 \times \text{diag}([1, 1, 3]) \tag{88b}$$

The initial state covariance matrix was constructed assuming an initial attitude uncertainty of 20 deg about X and Y and 180 deg about Z and a rate uncertainty of 10 deg/s on each axis. The simulation time span is 25 min and is centered on perigee, where the altitude is low enough for the TAM data to be useful. The first 3 min of each run are discarded from the results to allow time for the filter transients to damp out.

B. Test Results

The values reported in this section are a measure of the spin axis pointing error, which is the root sum square of the X- and Y-axis errors obtained by converting the filter state vector estimates into equivalent quaternions, comparing with the truth-model quaternions, and determining the root-mean-square error about each axis. The spin phase error is not reported because science instrument data for which the phase is important are generally tagged by a sun pulse time plus some delta time, so that the long time history of the phase is not important and should not be included in the statistics of the results.

A series of tests was designed to stress the filters in four different ways: reducing the number of observations per spin period, increasing the propagation step size, increasing the initial attitude error, and increasing the error in the inertia tensor model.

Before these stressing cases, four baseline scenarios were tested to verify filter performance with parameters similar to those used for operational support of THEMIS. The nominal scenario consists of torque-free motion, a 2-deg nutation angle, no sensor misalignments, an accurately modeled inertia tensor, and uses TAM data (24 per spin period) and sun sensor data (one per spin period). The second scenario was the nominal scenario with two-axis gyro data added. The third scenario was the same as the nominal scenario, but with misalignments of 0.1 deg on the TAM and sun sensor. The fourth scenario was also similar to the nominal, but with a torque applied in the body frame for 10% of each spin period to precess the spin axis by 30 deg during the 25-min time span. Note that the filter is *not* given the torque values for any of the tests presented here; if the torque values are passed to the filter, the filter will agree very closely with the truth model (the errors then are indistinguishable from the nominal case).

Table 1 shows the results of these first tests for SpinKF1, SpinKF-B, SpinKF-I, and the UVF. In these tests, the initial attitude errors relative to the truth model are 10 deg about the X and Y axes and 45 deg about Z, and the rate errors are 5 deg/s about X and Y and 10 deg/s about Z. As a measure of computational burden, the mean clock times for these runs are 47, 25, 25, and 26 s for SpinKF1, SpinKF-B, SpinKF-I, and the UVF, respectively. These times are platform-dependent, but the relative times are significant. SpinKF1 is slower, in part because its partial derivative expressions are much

Table 1 Results of baseline filter tests

Scenario	SpinKF1 pointing error, deg	SpinKF-B pointing error, deg	SpinKF-I pointing error, deg	UVF pointing error, deg
Nominal	0.0810	0.0873	0.0874	0.0873
Nominal plus gyro	0.0769	0.0249	0.0249	0.0249
Misaligned sensors	0.1325	0.1387	0.1390	0.1392
30-deg slew (no torque data to KF)	0.1142	0.7139	0.7348	0.7110

Table 2 Filter test results with TAM data frequency reduced to 2.1 observations per spin period

Scenario	SpinKF1 pointing error, deg	SpinKF-B pointing error, deg	SpinKF-I pointing error, deg	UVF pointing error, deg
Nominal	0.1171	0.1097	0.1098	0.1097
Nominal plus gyro	0.1120	0.0367	0.0370	0.0367
Misaligned sensors	0.1596	0.1538	0.1537	0.1538
30-deg slew (no torque data to KF)	0.1625	1.2662	1.2654	1.2764

more complicated than the other filters, but also because its MATLAB code has not been as thoroughly optimized.

It is clear from Table 1 that all five filters are performing well and are in good agreement, except that SpinKF1 performs better than the other filters with the attitude slew, but not as well when gyro data are included. We were unable to determine the cause of these performance differences.

The next set of tests examines how the filters respond with reduced data availability. Table 2 shows results for the same four scenarios as in Table 1, but with the TAM data frequency reduced from 24 to 2.1 observations per spin period. (The number is deliberately nonintegral so that the spin phase at the TAM measurement times will not be constant.) The propagation step size was set to $\frac{1}{8}$ s to match the step size in the baseline tests (driven in that case by the TAM frequency). With fewer data, the attitude errors shown in Table 2 are larger than those in Table 1, but the filters still perform well. When the TAM frequency is reduced further, all the filters tend to diverge, depending largely on the chance transients from the first few data points.

The filter determines the propagation step size first, from the data time steps, and second, from an input parameter that specifies a maximum allowed time step. Whenever the time between observations is larger than this maximum step size, additional integration steps are inserted as required. To test the numerical propagation, the next test increased the maximum allowed step size while keeping the actual data frequency low. With the TAM frequency at 2.1 observations per spin period and the maximum step size equal to 0.5 s, all the filters except SpinKF1 and SpinKF-I begin to fail the test scenarios. Table 3 shows that increasing the step size further to 0.7 s causes SpinKF-I to fail in some cases, but displays no clear pattern. The convergence region is small for all the filters when the data are sparse and the propagation step size is large. Whether a filter diverges or not then is largely just a happenstance caused by the first few data points. If the transients push the state far enough from the truth so that nonlinearities in the sensor models become important, the filter often never recovers. When the step size is increased to 1 s, SpinKF1 also diverges.

The next series of tests considers the effect of varying the initial attitude error in the nominal scenario (torque-free, 2-deg nutation, 8 Hz TAM, no misalignments, and $\frac{1}{8}$-s propagation step size). The initial rate error is kept at 5 deg/s about X and Y and 10 deg/s about Z. Table 4 shows selected results. Entries with relatively large values indicate cases where the filter did converge but took longer than 3 min to settle down to linear behavior, and so some of the initial transients are included in the statistics. The results are mixed, but it is clear the SpinKF filters do not outperform the UVF when presented with large initial errors.

The last row in Table 4 shows that all four filters converged when the X and Y errors were zero and the Z error was large: that is, with spin phase error only. The initial spin phase is typically completely unknown. Experience with many runs with simulations and actual flight data shows that occasional filter divergence can be expected even when the initial pointing direction is known to within a few degrees. When this happens, restarting the filter with the phase shifted by 180 deg almost always gives a good solution. To avoid these occasional unnecessary divergences, the filter could self-initialize by making a rough attitude estimate using data from the first few spin periods. This feature will be added to the operational version of the filter in a future release.

The final set of tests is again based on the nominal scenario, but now includes various amounts of error in the inertia tensor. The simulator uses the inertia given by Eq. (87) in all cases, but the filter here is given an incorrect inertia for propagation. The first row in Table 5 uses an inertia tensor close to the actual value for THEMIS after TAM boom deployment. In this case, all the filters except SpinKF1 show similar errors of only 1.1 deg. The errors are relatively small here because the inertia tensor error consists primarily of a rotation of the principal-axis frame about the nominal body-frame Z axis by about 41 deg with only 0.15-deg X and Y rotation. The 41-deg Z rotation has no significant effect because the truth-model inertia tensor is axisymmetric. The combined X and Y rotation tips the major principal axis away from the body Z axis, which induces coning motion into the propagation that is not present in the truth-model

Table 3 Filter test results with TAM data frequency reduced to 2.1 observations per spin period and the maximum propagation step size increased to 0.7 s

Scenario	SpinKF1 pointing error, deg	SpinKF-B pointing error, deg	SpinKF-I pointing error, deg	UVF pointing error, deg
Nominal	0.7027	Diverged	Diverged	Diverged
Misaligned sensors	0.7115	Diverged	0.1816	Diverged
30-deg slew (no torque data to KF)	0.1631	1.4762	1.2690	Diverged

Table 4 Filter results for nominal scenario with various initial attitude errors

Initial attitude errors, deg	SpinKF1 pointing error, deg	SpinKF-B pointing error, deg	SpinKF-I pointing error, deg	UVF pointing error, deg
$X\text{err} = 30$, $Y\text{err} = 30$, $Z\text{err} = 0$	0.0802	0.0873	0.0874	0.0873
$X\text{err} = 60$, $Y\text{err} = 60$, $Z\text{err} = 0$	0.0802	3.1932	0.1119	0.0873
$X\text{err} = 80$, $Y\text{err} = 80$, $Z\text{err} = 0$	Diverged	14.4281	Diverged	0.1199
$X\text{err} = 90$, $Y\text{err} = 0$, $Z\text{err} = 0$	0.0808	0.0873	0.0874	0.0873
$X_{\text{err}} = -90 Y\text{err} = 0$, $Z\text{err} = 0$	0.0810	0.0891	0.0874	0.0873
$X\text{err} = 120$, $Y\text{err} = 0$, $Z\text{err} = 0$	0.0810	Diverged	0.0875	0.0874
$X\text{err} = 0$, $Y\text{err} = 120$, $Z\text{err} = 0$	Diverged	Diverged	Diverged	Diverged
$X\text{err} = 170$, $Y\text{err} = 0$, $Z\text{err} = 0$	11.2017	0.0873	Diverged	Diverged
$X_{\text{err}} = -170 Y\text{err} = 0$, $Z\text{err} = 0$	3.7612	Diverged	0.0876	Diverged
$X\text{err} = 30$, $Y\text{err} = 30$, $Z\text{err} = -175$	0.0804	0.0833	Diverged	0.0815
$X\text{err} = 0$, $Y\text{err} = 0$, $Z\text{err} = 175$	0.0807	0.0875	0.0881	0.0873

Table 5 Filter results for nominal scenario with various errors in the inertia tensor

Inertia tensor, kg-m^2	SpinKF1 pointing error, deg	SpinKF-B pointing error, deg	SpinKF-I pointing error, deg	UVF pointing error, deg
$J_{\text{EKF}} = \begin{bmatrix} 12.4 & -5.3 & -.02 \\ -5.3 & 14.0 & -.01 \\ -.02 & -.01 & 21.7 \end{bmatrix}$	1.9872	1.1134	1.1164	1.1137
$J_{\text{EKF}} = \begin{bmatrix} 12.4 & -2 & -1 \\ -2 & 14.0 & 0 \\ -1 & 0 & 21.7 \end{bmatrix}$	7.4997	7.0813	6.8028	7.3736
$J_{\text{EKF}} = \begin{bmatrix} 14 & 0 & -1.5 \\ 0 & 12 & 0 \\ -1.5 & 0 & 22 \end{bmatrix}$	11.9418	14.5196	10.5923	13.7981
$J_{\text{EKF}} = \begin{bmatrix} 14 & -2 & -2 \\ -2 & 12 & 0 \\ -2 & 0 & 22 \end{bmatrix}$	15.9104	30.1164	13.9457	38.6044

attitude. However, a larger source of error in this example is that this tensor is far from axially symmetric, and so the nutational motion is not predicted accurately. The eigenvalues of J are approximately 7.8, 18.5, and 21.7 kg-m^2; the lack of symmetry is indicated by the difference between the first and second eigenvalues not being small relative to the third.

In the second case in Table 5, the principal-axis frame is tipped by 6.6 deg from the body frame. Compared with the first case, the symmetry error is less important because the eigenvalues are 11.0, 15.3, and 21.8 kg-m^2. Thus, the coning error predominates. In the third and fourth cases in Table 5, the principal-axis frame is tipped by 10.3 and 14.1 deg, respectively, and again, coning error predominates. As the coning angle increases, the SpinKF-I error follows it closely, but the other filters begin to show larger errors. The covariance propagation is probably more accurate for SpinKF-I because it uses $\Delta\mathbf{L}_I$ rather than $\Delta\mathbf{L}_B$ in its error state vector. Specifically, the lower half of F_{yI} in Eq. (62a) does not include a factor of J, and so this part of the covariance propagation is not corrupted by the error in the inertia tensor.

IX. Estimation Results with Flight Data

Ground support for the five THEMIS probes used the earlier version of the SpinKF described in [13]. Based on the preceding simulation results, this was replaced by SpinKF-I, which now has been fully integrated into the ground support software used for mission support at the NASA Goddard Space Flight Center. Samples of THEMIS flight data were reprocessed using SpinKF-I. The difference between these results and those of [13] is oscillatory with a magnitude of roughly 60 arc seconds and is indistinguishable on typical plots.

Before filter performance could be assessed, the sensors needed to be calibrated. In particular, the TAM was deployed after launch on a 2-m boom and has an alignment uncertainty of approximately 1 deg. The calibration utility uses an attitude-independent method [25] to determine biases, scale factors, and skewness of the axes and uses an iterative method [26] to determine the orthogonal sensor alignment. SpinKF-I is a key part of the iterative method. The calibrations were repeated several times for each probe using data sets from March 2007. Each data span covers 50 to 60 min near perigee. The reference magnetic field was obtained using the IGRF 2005 model to tenth order, along with definitive ephemerides for the spacecraft positions.

The spacecraft attitude history was determined using SpinKF-I before and after calibration. Before calibration, the sensor residuals from the filter show offsets of 1 to 2 deg from zero, primarily due to misalignment. Calibration removes these offsets and reduces their standard deviations by up to a factor of 2.

The spin vector is nominally aligned with the body Z axis and is constant in an inertial frame; however, a nonzero coning angle is

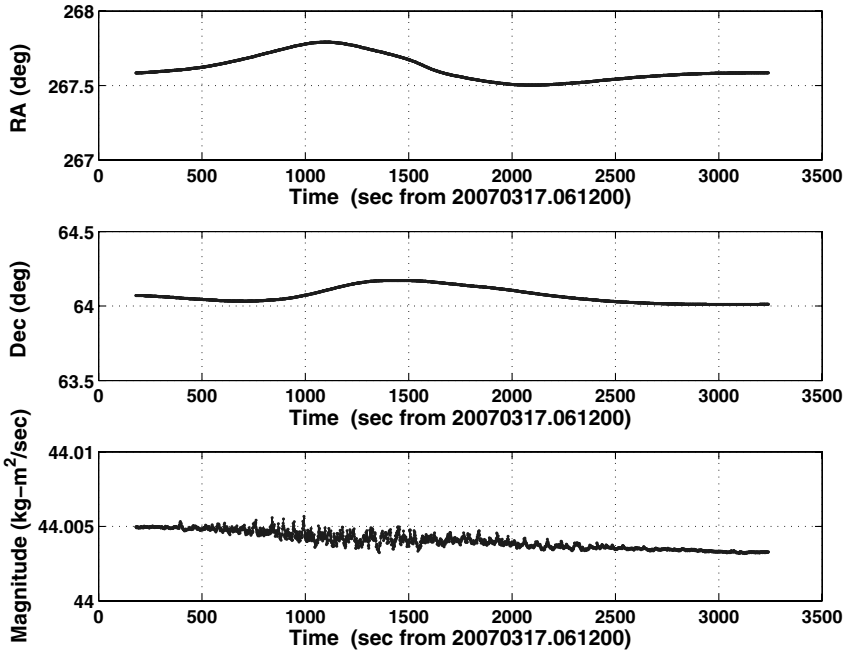

Fig. 1 Right ascension, declination, and magnitude of the angular momentum vector estimated using SpinKF-I for THEMIS probe A after calibration of the magnetometer.

expected, especially before deployment of the radial wire booms. The calibration reduces the standard deviation of the Z-axis pointing direction by roughly a factor of 2, yielding a postcalibration 3-sigma Z-axis uncertainty of 0.4 to 0.5 deg for probes A–D and 0.7 deg for probe–E. This is in excellent agreement with the Z-axis coning motion predicted from the inertia tensors. The angular momentum direction is more nearly constant; it does not vary due to coning. The angular momentum direction 3-sigma uncertainties range from less than 0.1 to 0.3 deg for all postcalibration solutions for the five probes.

Figure 1 shows a typical solution for the estimated angular momentum right ascension, declination, and magnitude for probe A. The variation in the angular momentum direction seen in Fig. 1 is not physical. Gravity gradient is the largest environmental torque, and it precesses the angular momentum vector by only 0.01 deg per orbit, much less than the variation seen in Fig. 1. It is likely that a reference magnetic field error due to a small, but not entirely negligible, ephemeris error causes this small variation. This problem was seen, greatly exaggerated, early in the mission before accurate ephemerides were available. On the other hand, the apparent slow downward drift of the angular momentum magnitude results from cooling of onboard fuel that, being forced to the outer edge of the tanks, contracts away from the spin axis, thereby increasing the moment of inertia about that axis and decreasing the spin rate. Assuming a constant inertia tensor, the filter misinterprets this as a decreasing angular momentum.

X. Conclusions

A class of extended Kalman filters for spinning spacecraft was developed using a seven-component angular-momentum-based attitude parameterization. The state vector is constrained by the requirement that the magnitude of the angular momentum is the same in all reference frames, allowing the filters to employ a six-component error state instead of the error vector of the full seven-component state. This is similar to the procedure commonly used to estimate the constrained four-component quaternion representation of attitude. Different filters in this class all use the same seven-component state but differ in their specification of the six-component error state. The error states of the two filters introduced in this paper comprise the vector of infinitesimal attitude error angles and the angular momentum vector in either the spacecraft body frame (SpinKF-B) or in an inertial frame (SpinKF-I).

These filters were tested against a conventional quaternion-based filter, using data simulated to represent a spacecraft of the THEMIS mission. A nominal test was performed for torque-free motion, with a 2-deg nutation angle, no sensor misalignments, an accurately modeled inertia tensor, three-axis magnetometer data, and sun sensor data. Three variations on this nominal test were run by adding gyro data, misaligning the magnetometer and sun sensor by 0.1 deg, and applying a torque to precess the spin axis by 30 deg. The filter was not given the torque values for any of the tests, because that would have resulted in estimation errors indistinguishable from the nominal case. The performance of the filters was virtually identical in this series of tests, with the exception that the oldest version of the filter, SpinKF1, performed significantly better in the 30-deg slew case. The reason for this is unknown, and the execution time of this filter was almost twice as great as that of SpinKF-B or SpinKF-I, in part because its partial derivative expressions are much more complicated, but also because its code has not been as thoroughly optimized. The four filters would have all performed equally well in the 30-deg slew case if they had been provided with perfect torque information.

This baseline set of cases was followed by a series of tests designed to stress the filters in four different ways: reducing the number of observations per spin period, increasing the propagation step size, increasing the initial attitude error, and increasing the error in the modeled moment-of-inertia tensor. None of the filters exhibited a clear superiority in these tests, but the SpinKF filters generally outperformed the quaternion-based filter for the largest step size, and SpinKF-I was least corrupted by errors in the inertia tensor. On balance, SpinKF-I showed the best combination of robustness and efficiency in the simulations, and so it has now been fully integrated into the ground support software used for mission support at NASA Goddard Space Flight Center.

Appendix: SpinKF1

SpinKF1 uses the seven-component state vector

$$\mathbf{x} = [\hat{\mathbf{L}}_I^T \quad \mathbf{L}_B^T \quad \zeta]^T \tag{A1}$$

This differs from Eq. (12) in using the unit vector $\hat{\mathbf{L}}_I$ in place of $\mathbf{L}_I$ and in an unimportant transposition of components. The constraint on this state vector is not Eq. (3), but $\|\hat{\mathbf{L}}_I\| = 1$. Thus, the null vector is

$$\mathbf{x}_{\text{null}} = \pm[\hat{\mathbf{L}}_I^T \quad 0_{1\times 4}]^T \tag{A2}$$

Equations (15) and (16) are satisfied by

$$S_1^+ = S_1^T = \begin{bmatrix} \begin{bmatrix} 1 & 0 & 0 \\ 0 & 1 & 0 \end{bmatrix} R_{\mathbf{z}I} & 0_{2\times 4} \\ 0_{4\times 3} & I_{4\times 4} \end{bmatrix} \tag{A3}$$

where

$$R_{\mathbf{z}I} = (\hat{\mathbf{z}}\cdot\hat{\mathbf{L}}_I)I_{3\times 3} - \hat{\mathbf{L}}_I\hat{\mathbf{z}}^T + \hat{\mathbf{z}}\hat{\mathbf{L}}_I^T + (1+\hat{\mathbf{z}}\cdot\hat{\mathbf{L}}_I)^{-1}(\hat{\mathbf{z}}\times\hat{\mathbf{L}}_I)(\hat{\mathbf{z}}\times\hat{\mathbf{L}}_I)^T \tag{A4}$$

is a rotation matrix that takes $\hat{\mathbf{L}}_I$ into $\hat{\mathbf{z}} \equiv [0 \quad 0 \quad 1]^T$. The six-dimensional EKF follows the same pattern as the other versions of SpinKF, except that the state renormalization after the measurement update is equivalent to

$$\bar{\hat{\mathbf{L}}}_I(++) = \bar{\hat{\mathbf{L}}}_I(+)/\|\bar{\hat{\mathbf{L}}}_I(+)\| \tag{A5}$$

The computation of the measurement sensitivity matrices in SpinKF1 is more difficult than in the other versions of SpinKF, because the infinitesimal attitude error angles are not part of the reduced error vector. SpinKF1 also contains a singularity when $\mathbf{L}_I$ and $\hat{\mathbf{z}}$ are 180 deg apart that is not present in the other filters. This singularity is handled in the same way by redefining the inertial reference frame. SpinKF1 is described in detail in [10].

References

[1] Markley, F. L., "New Dynamic Variables for Momentum-Bias Spacecraft," *Journal of the Astronautical Sciences*, Vol. 41, No. 4, 1993, pp. 557–567.

[2] Lefferts, E. J., Markley, F. L., and Shuster, M. D., "Kalman Filtering for Spacecraft Attitude Estimation," *Journal of Guidance, Control, and Dynamics*, Vol. 5, No. 5, 1982, pp. 417–429.

[3] Markley, F. L., "Attitude Estimation or Quaternion Estimation?" *Journal of the Astronautical Sciences*, Vol. 52, Nos. 1–2, 2004, pp. 221–238.

[4] Shuster, Malcolm, D., "Constraint in Attitude Estimation Part 1: Constrained Estimation," *Journal of the Astronautical Sciences*, Vol. 51, No. 1, 2003, pp. 51–74.

[5] Shuster, Malcolm, D., "Constraint in Attitude Estimation Part 2: Unconstrained Estimation," *Journal of the Astronautical Sciences*, Vol. 51, No. 1, 2003, pp. 75–101.

[6] Pittelkau, M. E., "An Analysis of the Quaternion Attitude Determination Filter," *Journal of the Astronautical Sciences*, Vol. 51, No. 1, 2003, pp. 103–120.

[7] Zanetti, R., and Bishop, R. H., "Quaternion Estimation and Norm Constrained Kalman Filtering," AIAA/AAS Astrodynamics Specialist Conference, Keystone, CO, AIAA Paper No. 2006-6164, August 2006.

[8] Calise, A. J., "Enforcing an Algebraic Constraint in Extended Kalman Filter Design," AIAA Guidance, Navigation, and Control Conference, AIAA Paper No. 2006-6515, Hilton Head, SC, Aug. 2007.

[9] Carmi, A., and Oshman, Y., "On the Covariance Singularity of Quaternion Estimators," AIAA Guidance, Navigation, and Control Conference, AIAA Paper No. 2006-6814, Hilton Head, SC, Aug. 2007.

[10] Sedlak, J. E., "Spinning Spacecraft Attitude Estimation Using Markley Variables: Filter Implementation and Results," NASA Goddard Space Flight Center CP-2005-212789, Greenbelt, MD, Oct. 2005.

[11] Speer, D., Jackson, G., Stewart, K., and Hernandez-Pellerano, A., "The Space Technology 5 Avionics System," *2005 IEEE Aerospace Conference*, Inst. of Electrical and Electronics Engineers, Piscataway, NJ, Mar. 2005, pp. 768–780.

[12] Sedlak, J., Hashmall, J., Brasoveanu, D., Ottenstein, N., Glickman, J., and Carpenter, R., "Flight Dynamics (FD) Task Order 88, Spacecraft Attitude Determination Accuracy from Mission Experience," Rev. 1, Update 6, Honeywell Technology Solutions, Inc., Rept. FDF-88-021, Lanham, MD, Dec. 2006.

[13] Markley, F. L., and Sedlak, J. E., "Kalman Filtering of Angular-Momentum-Based Attitude Parameters," *7th Cranfield Conference on Dynamics and Control of Systems and Structures in Space*, edited by S. Hobbs, Cranfield Univ. Press, Cranfield, England, U.K., 2006.

[14] Donovan, E., Mende, S., Jackel, B., Frey, H., Syrjäsuo, M., Voronkov, I., Trondsen, T., Peticolas, L., Angelopoulos, V., Harris, S., Greffen, M., and Connors, M., "The THEMIS All-Sky Imaging Array—System Design and Initial Results from the Prototype Imager," *Journal of Atmospheric and Solar-Terrestrial Physics*, Vol. 68, No. 13, 2006, pp. 1472–1487. doi:10.1016/j.jastp.2005.03.027

[15] Wertz, J. R. (ed.), *Spacecraft Attitude Determination and Control*, D. Reidel, Dordrecht, The Netherlands, 1978, Chaps. 12 and 16.

[16] Humphreys, T. E., Psiaki, M. L., Klatt, E. M., Powell, S. P., and Kintner, P. M., "Magnetometer-Based Attitude and Rate Estimation for Spacecraft with Wire Booms," *Journal of Guidance, Control, and Dynamics*, Vol. 28, No. 4, 2005, pp. 584–593. doi:10.2514/1.7603

[17] Shuster, Malcolm, D., "A Survey of Attitude Representations," *Journal of the Astronautical Sciences*, Vol. 41, No. 4, 1993, pp. 439–517.

[18] Golub, G. H., and Van Loan, C. F., *Matrix Computations*, Johns Hopkins Univ. Press, Baltimore, MD, 1983, p. 139.

[19] Gelb, A. (ed.), *Applied Optimal Estimation*, MIT Press, Cambridge, MA, 1974.

[20] Reynolds, R. G., "Asymptotically Optimal Attitude Filtering with Guaranteed Convergence," *Journal of Guidance, Control, and Dynamics*, Vol. 31, No. 1, 2008, pp. 114–122.

[21] Sedlak, J., and Chu, D., "Kalman Filter Estimation of Attitude and Gyro Bias with the QUEST Observation Model," *Proceedings of the AAS/GSFC International Symposium on Space Flight Dynamics*, Greenbelt, MD, American Astronautical Society Paper 93-297, 1993.

[22] Reynolds, R. G., "Quaternion Parameterization and a Simple Algorithm for Global Attitude Estimation," *Journal of Guidance, Control, and Dynamics*, Vol. 21, No. 4, 1998, pp. 669–671.

[23] Markley, F. L., "Fast Quaternion Attitude Estimation from Two Vector Measurements," *Journal of Guidance, Control, and Dynamics*, Vol. 25, No. 2, 2002, pp. 411–414.

[24] Sedlak, J. E., "Improved Spacecraft Attitude Filter Using a Sequentially Correlated Magnetometer Noise Model," *16th AIAA/IEEE Digital Avionics Systems Conference*, Vol. 2, Inst. of Electrical and Electronics Engineers, Piscataway, NJ, Oct. 1997, pp. 8.4-9–8.4–16.

[25] Alonso, R., and Shuster, M. D., "Complete Linear Attitude-Independent Magnetometer Calibration," *Journal of the Astronautical Sciences*, Vol. 50, No. 4, 2002, pp. 477–490.

[26] Sedlak, J. E., "Iterative Magnetometer Calibration," AIAA/AAS Astrodynamics Specialist Conference, Keystone, CO, AIAA Paper No. 2006-6386, Aug. 2006.